Sixth International Symposium on Turbulence and Shear Flow Phenomena
Seoul, Korea, 22-24 June 2009

VISCOUS FLOW FEATURES IN SCALED-UP PHYSICAL MODELS OF NORMAL AND PATHOLOGICAL VOCAL PHONATION

Byron D. Erath
School of Mechanical Engineering,
Purdue University
585 Purdue Mall, West Lafayette, IN, 47907, USA
berath@purdue.edu

Michael W. Plesniak
Department of Mechanical and Aerospace Engineering
The George Washington University
801 22nd Street NW, Suite 739, Washington DC 20052, USA
plesniak@gwu.edu

ABSTRACT

Unilateral vocal fold paralysis results when the recurrent laryngeal nerve which innervates the muscles of the vocal folds becomes damaged. The loss of muscle and tension control to the damaged vocal fold renders it ineffectual. The mucosal wave disappears during phonation, and the fold becomes largely immobile. The influence of unilateral vocal fold paralysis on the viscous flow development within the glottis during phonation was investigated. Driven, scaled-up vocal fold models were employed to replicate both normal and pathological patterns of speech. Spatial and temporal velocity fields were captured using Particle Image Velocimetry, and laser Doppler velocimetry. Flow parameters were scaled to match the physiological values in human speech. Loss of motion in one vocal fold resulted in a suppression of typical glottal flow fields, including decreased variability in the flow separation point throughout the glottal cycle, as well as a decrease in the flow vorticity.

INTRODUCTION

Human vocal folds serve as the primary regulators of speech, oscillating as a result of coupling between the aerodynamic forces and tissue properties. During a typical phonation cycle the glottis, the space between the vocal folds, transitions from a convergent, to uniform, and then divergent channel before closing again. This complex motion is generated by a mucosal wave travelling along each facing medial vocal fold surface. The temporally-varying flow features which result from the vocal fold kinematics ultimately contribute to the sound which is produced during speech.

During normal phonation the dynamically-varying glottal geometry foments the development of rich viscous flow behavior, including varying flow separation points, the Coanda effect, glottal jet skewing, and turbulent flow transition.

Historically neglected in laryngeal flows (Hirschberg et al., 1996; Hofmans et al., 2003), recent investigations have highlighted the existence and importance of viscous flow features during normal phonation. Triep et al. (2005) investigated the supraglottal flow field in a driven model, indicating the tendency of the jet to skew from side to side. Erath and Plesniak, (2006a, 2006b) and Suh and Frankel (2007) performed complementary experimental and numerical investigations, respectively, showing that the Coanda effect occurs within the glottis in pulsatile flow through static vocal fold models. Additional supraglottal flow field investigations have been performed using excised canine larynges (Khosla et al., 2007), and self-oscillating vocal fold models (Neubauer et al., 2007; Drechsel and Thomson, 2008).

In spite of the recent studies of viscous flow behavior for normal phonation, there is a dearth of work quantifying pathological flow behavior within the glottis, largely due to the inaccessibility of *in-vivo* investigations, and the difficulty of replicating common neurological pathologies using physical models.

Neurological pathologies, such as unilateral vocal fold paralysis, hinder vocal fold motion, and severely impair speech quality. The recurrent laryngeal nerve (RLN) innervates all of the muscles of the larynx, except the cricothyroid. Damage to the RLN usually results in complete immobility of one vocal fold (Fex, 1970; Kitzing, 1985) although some studies have observed mucosal wave motion (albeit limited) along the paralyzed fold (Sercarz et al., 1992). Damage to the RLN most commonly occurs as a complication of thyroid surgery (Schwarz et al., 2006), but may also arise due to inflammation from infection, or pressure on the nerve from a tumor (Lo et al, 2000; Yumoto et al., 2002).

The objective of this work is to investigate the development of viscous flow features for both normal and pathological vocal fold motions caused by RLN paresis and paralysis.

EXPERIMENTAL APPARATUS

All experiments were performed in a pressure driven wind tunnel. Designed for laryngeal flow, low Reynolds number investigations, the pressure supply was generated by compressed air at ~100-120 psi. The pressure is

regulated through a Nullmatic 40-100 pressure regulator, before passing through a Dwyer Instruments rotameter which measures the volumetric flow rate. The air supply then branches with one line entering a TSI Laskin nozzle olive oil atomizer, and the other line rejoining at the exit of the atomizer. Needle valves control the respective flow through both lines, allowing adjustment of the seeding rate. Finally, the seeded air flow enters the wind tunnel through a backwards facing perforated 2.00 inch (5.08 cm) O.D. PVC pipe placed longitudinally to the flow direction. The wind tunnel consists of a settling chamber, honeycomb flow straighteners, and a contraction ratio of 4, designed according to the cubic matching point of Morel (1977). The test section measures 3.60 inches (9.14 cm) high in the longitudinal direction and 4.96 inches (12.60 cm) wide in the spanwise direction. The vocal folds are inserted such that the leading edge is 6.00 inches (15.24 cm) downstream of the entrance to the test section and oriented such that the anterior-posterior and medial-lateral *in-vivo* orientations are aligned with the longitudinal and spanwise directions, respectively.

The vocal folds are constructed according to the 2-D M5 geometry of Scherer et al. (2001), and scaled-up by 7.5. The medial surface, and inlet and exit radii are machined from aluminium. Latex attaches to the inlet and exit radii and the vocal fold walls, thereby forming the exterior shape of each vocal fold model. Each model has an internal bladder that is filled with water. As a result, as the vocal folds are abducted from their initial adducted state, the latex walls began to bulge, creating a vocal fold which is volume conserving, that is the total volume does not change throughout the vocal fold motion.

Motion control is achieved via a pair of two stepper motor/driver combinations. Each vocal fold is independently controlled by two stepper motors and drivers (Oriental Motors 400 oz-in, Velmex NF-90). One motor drives the linear motion in the medial-lateral direction, while the other controls the angular rotation of the medial surface. The center-of-rotation is about the midpoint of the medial surface, along the contact line of the two vocal folds. With compliance provided by the latex attachment points, the vocal fold models can be driven in a manner that replicates the mucosal wave as it propagates along the medial vocal fold surface. The programmable nature of the stepper motors allows both normal and pathological vocal fold motions to be replicated. An external trigger generated in LabView v8.2 initiates the motion, allowing the vocal fold movements to be synchronized with the data acquisition.

METHODS

Vocal Fold Motion

Vocal fold motions were prescribed for three cases. Normal phonation, RLN paresis with limited motion, and RLN paralysis with no motion. Reynolds number, Strouhal number, and pressure coefficient were scaled to match physiological values. Figure 1 shows the prescribed linear and angular motions of one vocal fold model for the case of normal phonation. Table 1 describes the pertinent motion parameters for each of the three cases where the open quotient (OQ) is defined as T_{open}/T_{cycle}, and the speed quotient (SQ) is defined as $T_{openinng}/T_{closing}$. The vocal fold identification (left/right) is specified from a superior viewpoint. Accordingly, the right fold is oriented in the positive y-direction, and the left fold in the negative y-direction. The vocal fold angle and position are both measured relative to the medial midline, and d is the maximum glottal gap.

Particle Image Velocimetry (PIV)

The spatial flow field was resolved within the glottal space along the anterior-posterior midline by employing phase-averaged PIV measurements. 1,050 image pairs were acquired at 9 phases throughout each cycle, labelled in figure 1 as points A – H. The laser light sheet was produced by a New Wave Gemini Laser Nd:YAG laser. Image pairs were acquired on a PowerView 4MP 2,000 x 2,000 pixel array CCD camera. TSI Insight 3G software handled timing, data acquisition, and vector processing. The images were interrogated on a recursive Nyquist grid (64 x 64, 32 x 32). An external trigger was used to begin acquisition, allowing synchronizing of various measurements.

Laser Doppler Velocimetry (LDV)

Instantaneous velocity traces of the supraglottal flow were obtained with a one-component Dantec Dynamics Flowlite 1D Laser Doppler Velocimeter (LDV). Dantec Dynamics BSA Flow Processing software was used for all signal processing. A linear profile of data was obtained from +1.50 cm to -1.50 cm in 0.25 cm increments, measured about the medial midplane. The measurement plane was at the anterior-posterior midplane, 1 cm superior to the glottal exit. Data from 250 cycles were acquired at each location.

Instantaneous Pressure Drop

Concurrent with the PIV measurements, the unsteady transglottal pressure drop was measured via two Validyne DP45-14 pressure transducers. Each transducer was short plumbed to a 0.125 inch (0.318 cm) diameter pressure tap. The upstream tap was placed 2.00 inches (5.08 cm) upstream of the leading edge of the vocal folds. The downstream tap was placed 1.50 inches (15.24 cm) downstream of the vocal fold exit. Data acquisition was performed with a National Instruments 6013 DAQ card at 3,000 samples/s. The TTL trigger initiated data acquisition, thereby synchronizing the vocal fold motion, PIV images, and the corresponding transglottal pressure trace for each cycle.

RESULTS

Instantaneous Velocity

The LDV temporal velocity traces are shown in figure 2. One diameter downstream from the glottal exit, the maximum velocity is approximately 2.2 m/s. The maximum velocity magnitude displays a similar temporal waveform reported in both physiological and in vitro experimental studies. A sharp acceleration upon glottal opening is followed by a relatively flat plateau. A secondary peak immediately preceding the sharp deceleration is identical to the behaviour reported by Mongeau et al. (1997).

Spatial Flow Fields

Glottal Jet Trajectory. Using the method of Erath and Plesniak (2006a) the gottal jet trajectory was calculated for each PIV velocity field realization during the closing phases (t/T_{open} = 0.50, 0.60, 0.70, 0.80, and 0.90) for the normal, paretic, and paralytic motion. The results are plotted in figure 3 – figure 5 as histograms, where α is the angle the glottal jet is deflected from the midline, and $\Psi/2$ is the vocal fold angular deflection for the case of normal motion (15^o). The early phases (0.30, and 0.40) are not shown due to the unvarying symmetric behaviour of the jet.

For the normal vocal fold motion (figure 3) the jet trajectory was similar to previously reported investigations (Triep et al., 2005; Erath and Plesniak, 2006a,b; Neubauer et al., 2007). During the divergent portion of the cycle, the initially undeflected jet is observed to randomly skew towards either vocal fold wall, and attach to it. However, attachment predominantly occurs later in the phonatory cycle than previously proposed (see Hofmans et al., 2003; Erath and Plesniak, 2006b). It was initially suggested that the formation of the Coanda effect may occur when the unsteady acceleration first approaches zero, that is, when the velocity reaches a steady state. Returning to the unsteady velocity traces of figure 2, this occurs at a time of approximately t/T_{open} = 0.4. However, as the glottis begins to form into a divergent channel, the flow remains largely symmetric until a phase of t/T_{open} = 0.7, at which point attachment occurs. Additionally, once attached, the flow appears to remain attached to one wall, even when the included glottal angle is 30 degrees, i.e., larger than the post-critical stalled diffuser angle for which pulsatile flow does not attach to static vocal fold models.

For the RLN paresis investigations with limited motion of the right vocal fold the jet trajectory is skewed slightly towards the left wall during the phases t/T_{open} = 0.6, and 0.7. While not attached to either wall, the jet is skewed to the extent that it remains symmetric relative to the channel orientation. Attaching to the impaired wall later in the cycle, the flow then remains stationary throughout the remainder of the cycle. Attachment occurs once the divergence angle begins decreasing (see figure 1).

Figure 5 shows the jet trajectory for the case of unilateral RLN paralysis. The jet trajectory shows almost no variations throughout the phonation cycle and remains attached to the paralytic wall throughout the entire cycle.

Velocity Fluctuations. Figure 6 shows vorticity magnitude plots for the three phonatory motions at t/T_{open} = 0.70. To avoid averaging out any flow features, the phase-averaged vorticity fields were created by averaging only those files corresponding to the dominant jet trajectory of figures 3 - 5 for each case. The vorticity magnitude is clearly influenced by the pathological motion with the magnitude of the impaired motion roughly half of that produced during normal vocal fold motion. Additionally, there is much more predominant vortex formation within the glottis.

The existence of vortex shedding along the medial surface (and as it is convected downstream) can be observed. The repeatable, periodic nature at which this occurs within the glottis is an important finding. Previous investigations (Kucinschi et al., 2006) have observed vortex shedding, downstream of the glottis, but not periodically developing structures within the glottis. Krane (2005) showed that the dipole sound source will be influenced by vortices passing through area variations, not only by coming in contact with surfaces of the vocal tract. This periodic formation of vortices would be expected to contribute to a tonal quality of sound within the vocal tract. It may further excite the pressure field like a Helmholtz resonator as the vortices pass over the gap between the true, and ventricular fold, similar to the additional sound source that Zhang et al. (2002) identified due to the glottal jet's interaction with this cavity.

Flow Separation. The phase-averaged velocity fields at the prevalent jet deflection angle for the three vocal fold motions are shown in figures 7 – 9. Velocity magnitude is plotted with superimposed streamlines. For both the normal and paretic motion, the flow separation point moves down the medial vocal fold surface towards the minimal constriction as the vocal folds begin to close (Points D and E). As the angular rotation of the vocal folds begins to decrease (see figure 1 for reference) the flow completely attaches to one vocal fold wall while separating from the opposing wall at the minimal glottal diameter. The separation point on the opposing wall, to which the flow is not attached, appears to remain relatively unchanged for the remainder of the cycle. The case of unilateral paralysis exhibits significantly different flow behavior. Initially attached to the immobile wall, the flow never detaches, and the flow separation points remain constant throughout the entire cycle.

For all three vocal fold motions, vortex shedding from the medial vocal fold surface within the glottis is observed. The presence of vortices in the flow field following the phase-averaging of the various realizations indicates the vortices are shed in a predictable, periodic manner.

Transglottal Pressure Drop. Table 2 shows the instantaneous transglottal pressure drop for each of the vocal fold motions as a function of the jet deflection angle. The reported pressure drop is the scaled-up life-size value. The transglottal pressure drop increases for the instances in which the flow attaches to a vocal fold wall, regardless of the wall orientation (for normal and impaired motion). The case of complete paralysis shows a minimal change. However, this can be attributed to the minimal change in jet divergence angle for the paralyzed motion. Had data existed for a larger jet deflection angle of θ = -7.5^o (meaning the flow would be symmetrically oriented between the vocal fold walls) it is anticipated the change in transglottal pressure drop would have decreased accordingly.

While the absolute pressure drop varied as a function of vocal fold motion, this trend should not be considered since the vocal fold motion is prescribed about the midline of the medial surface. Since all data were acquired at the same instance, the linear displacement was the same for all instances. However the total included divergence angle varies, resulting in a decrease in the minimal glottal diameter with increasing included divergence angle, and a subsequent increase in the transglottal pressure drop.

DISCUSSION

The flow behavior presented here for both normal, paretic, and unilateral paralytic motion demonstrates the importance of vocal fold motion related to the unsteady nature of glottal flows. During normal vocal fold motion, the glottal jet was shown to be highly erratic, as has been reported in previous laryngeal investigations. However, even with limited mobility of the damaged vocal fold, similar flow patters were identified, albeit on a diminished scale. In contrast, unilateral paralysis completely restricts the glottal jet behavior. In particular, changes in the flow separation points are not present throughout the cycle, and the vorticity magnitude is similarly reduced relative to the normal vocal fold motion.

It is expected that unilateral paralysis will affect the speech signal due to the preclusion of changing separation points, and vortex formation within the glottis. Mid-cycle changes in the separation point have been shown to affect the transglottal pressure drop during the phonatory cycle. Employing the acoustical analogy of Ffowcs-Williams and Hawkings (1969) it can be shown that for confined flows with moving boundaries, the dipole contribution can be directly correlated with the unsteady transglottal pressure drop (Zhao et al., 2002). Although the effect of flow orientation on the transglottal pressure drop was small, further studies should be performed to investigate the phenomenon at varying flow rates.

Most incidences of unilateral paralysis are treated by structural intervention in order to position the damaged vocal fold closer to the medial surface of the undamaged fold. The motivation for this treatment is to facilitate complete closure of the vocal folds during phonation. The ability to not only ensure closure, but also to restore some degree of motion within the damaged vocal fold may result in significant improvement in voice quality. Small degrees of motion within the damaged fold excited the flow instabilities resulting in changing flow separation points due to the development of the Coanda effect within the glottis.

It should be noted that these results are obtained for a driven two-dimensional vocal fold model. These results are limited in that the driven vocal fold motion is not a result of self-sustained oscillations, and the flow is strictly two-dimensional. While the assumption of two-dimensional flow is a reasonable approximation due to the high aspect ratio of the glottis, the effect of driven versus self-sustained oscillations on the development of the flow field is unknown. Wall motion has been shown to be important in the development of vortical structures within the glottis, as well as in changing the separation phenomena of the glottal jet. It remains to be examined how these results correlate with self-oscillating models.

CONCLUSIONS

The intraglottal flow field has been investigated in a mechanically driven scaled-up vocal fold model for both normal and pathological vocal fold motion due to unilateral RLN paralysis. Temporal and spatial velocity fields for normal motion exhibit similar flow features to published experimental investigations, validating the model. The occurrence of periodic vortex shedding within the glottis has been observed for both normal and pathological vocal fold motions. It has been shown that decreased vocal fold motions due to paresis and paralysis stabilize the glottal jet trajectories, thereby suppressing flow separation point variations along the medial vocal fold surface due to flow asymmetries. Additionally it was shown that for impaired motion of one vocal fold, the RMS velocity fluctuations and vorticity field magnitudes are greatly reduced.

ACKNOWLEDGEMENTS

This research was supported by Grant #CBET-0828903 from the Division of Chemical, Bioengineering, Environmental, and Transport Systems (CBET), National Science Foundation.

REFERENCES

Drechsel, J., S., and Thomson, S. L., 2008, "Influence of Supraglottal Structures on the Glottal Jet Exiting a Two-Layer Synthetic, Self-Oscillating Vocal Fold Model," *Journal of the Acoustical Society of America*, Vol. 123, pp. 4434–4445.

Erath., B. D., and Plesniak, M. W., 2006a, "An Investigation of Bimodal Jet Trajectory in Flow Through Scaled Models of the Human Vocal Tract," *Experiments in Fluids*, Vol. 40, pp. 683-696.

Erath, B. D., and Plesniak, M. W., 2006b, " The Occurrence of the Coanda Effect in Pulsatile Flow Through Static Models of the Human Vocal Folds," *Journal of the Acoustical Society of America,* Vol. 120: 1000-1011.

Fex, S., 1970, "Judging the Movements of Vocal Cords in Larynx Paralysis," *Acta Otolaryngologica*, Vol. 263 (supplemental) pp. 82-83.

Ffowcs Williams, J. E., and Hawkings, D. L., 1969, "Sound Generation by Turbulence and Surfaces in Arbitrary Motion," *Philosophical Transactions of the Royal Society of London A*, Vol. 264, pp. 321-342.

Hirschberg, A., Pelorson, X., Hofmans, G.C.J., van Hassel, R.R., Wijnands, A.P.J., 1996, "Starting Transient of the Flow Through an *in-vitro* Model of the Vocal Folds," *Vocal Fold Physiology: Controlling Complexity and Chaos*, Davis, P.J., and Fletcher, N.H., ed., Singular Publishing Group, San Diego, CA, pp. 31-46.

Hofmans, G. C. J. , Groot, G., Ranucci, M., Graziani, G., and Hirschberg, A., 2003, "Unsteady Flow Through *in-vitro* Models of the Glottis," *Journal of the Acoustical Society of America*, Vol. 113, pp. 1658-1675.

Khosla, S., Muruguppan, S., Gutmark, E., and Scherer, R.C., 2007, "Vortical Flow Field During Phonation in an Excised Canine Larynx Model," *Annals of Otology Rhinology and Laryngology*, Vol. 116, pp. 217-228.

Krane, M. H., 2005, "Aeroacoustic Production of Low-Frequency Unvoiced Speech Sounds," *Journal of the Acousical Society of America*, Vol. 188, pp. 410-427.

Kucinshchi, B. R., Scherer, R. C., DeWitt, K. J., and Ng, T. T. M., 2006, "Flow Visualization and Acoustic Consequences of the Air Moving Through a Static Model of the Human Larynx," *Journal of Biomechanical Engineering*, Vol. 128, pp. 380-390.

Lo, C. Y., Kwok, K. F., and Yuen, P. W., 2000, "A Prospective Evaluation of Recurrent Laryngeal Nerve Paralysis During Thyroidectomy," *Archives of Surgery*, Vol. 135, pp. 204-207.

Mongeau, L., Franchek, N., Coker, C. H., and Kubli, R. A., 1997, "Characteristics of a Pulsating Jet Through a Small Modulated Orifice, With Application to Voice Production," *Journal of the Acoustical Society of America*, Vol. 102, pp. 1121-1133.

Morel, T., 1977, "Design of Two-Dimensional Wind Tunnel Contractions," *Journal of Fluids Engineering*, Vol. 99, pp. 371-378.

Neubauer, J., Zhang, Z., Miraghaie, R., and Berry, D., 2007, "Coherent Structures of the Near Field Flow in Self-Oscillating Physical Model of the Vocal Folds," *Journal of the Acoustical Society of America*, Vol. 121, pp. 1102-1118.

Scherer, R. C., Shinwari, D., DeWitt, K. J., Zhang, C., Kucinshi, B. R., and Afjeh, A. A., "Intraglottal Pressure Profiles for a Symmetric and Oblique Glottis with a Divergence Angle of 10 Degrees," *Journal of the Acoustical Society of America*, Vol. 109, pp. 1616-1630.

Schwarz, R., Hoppe, U., Schuster, M., Wurzbacher, T., Eysholdt, U., and Lohscheller, J., 2006, "Classification of Unilateral Vocal Fold Paralysis by Endoscopic Digital High-Speed Recordings and Inversion of a Biomechanical Model, *IEEE Transactions on Biomedical Engineering*, Vol. 53, pp. 1099-1108.

Sercarz, J. A., Berke, G. S., Gerrat, B. R., Ming, Y., and Natividad, M., 1992, "Videostroboscopy of Human Vocal Fold Paralysis," *Annals of Otology, Rhinology, and Laryngology*, Vol. 101, 567-576.

Suh, J., and Frankel, S. H., 2007, "Numerical Simulation of Turbulence Transition and Sound Radiation for Flow Through a Rigid Glottal Model," *Journal of the Acoustical Society of America*, Vol. 121, pp. 3728-3739.

Triep, M., Brucker, Ch., Schroder, W., 2005, "High-Speed PIV Measurements of the Flow Downstream of a Dynamic Mechanical Model of the Human Vocal Folds," *Experiments in Fluids*, Vol. 39, pp. 232-245.

Yumoto, E., Minoda, R., Hyodo, M., and Tamagata, T., 2002, "Causes of Recurrent Laryngeal Nerve Paralysis," *Auris Nasus Larynx*, Vol. 29, pp. 41-45.

Zhang, C., Zhao, W., Frankel, S. H., and Mongeau, L., 2002, "Computational Aeroacoustics of Phonation Part II: Effects of Flow Parameters and Ventricular Folds," *Journal of the Acoustical Society of America*, Vol. 112, pp. 2147-2154.

Zhao, W., Zhang, C., Frankel, S. H., and Mongeau, L., 2002, "Computational Aeroacoustics of Phonation, Part I: Computational Methods and Sound Generation Mechanisms," *Journal of the Acoustical Society of America*, Vol. 112, pp. 2134-2146.

Table 1: Parameters governing vocal fold motion

	Model			Physiological
	Normal	**Paretic**	**Paralytic**	
Left Fold				
d	*5.0*	*8.0*	*10.0*	*~0.3 - 1.0*
θ_{max}	*15*	*15*	*15*	*~10 - 20*
Right Fold				
d	*5.0*	*2.0*	*0.0*	*~0.3 - 1.0*
θ_{max}	*15*	*4*	*0*	*~10 - 20*
Re	*4,000*	*4,000*	*4,000*	*~2,000-5,000*
OQ	*0.6*	*0.6*	*0.6*	*0.5 - 0.9*
SQ	*1.0*	*1.0*	*1.0*	*0.6 - 1.0*
Frequency	*1.67*	*1.67*	*1.67*	*~100 - 250*

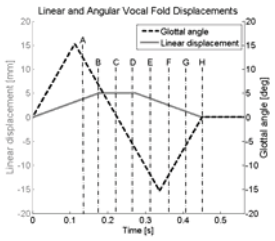

Figure 1: Linear and angular vocal fold displacements for normal vocal fold motion.

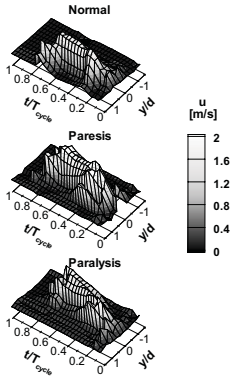

Figure 2: Temporal velocity traces throughout one vocal fold cycle for normal, paretic, and paralytic vocal fold motion.

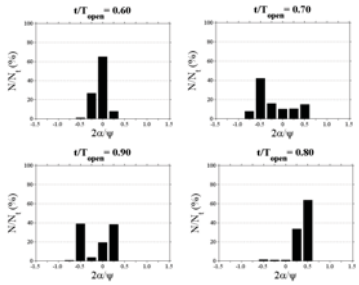

Figure 3: Glottal jet trajectory for normal vocal fold motion. α = jet deflection angle, Ψ = total included divergence angle for unimpaired motion (30°).

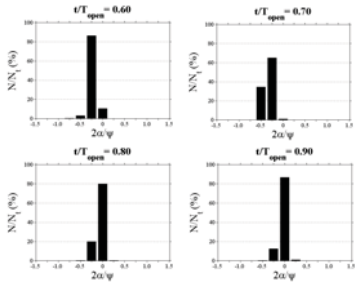

Figure 4: Glottal jet trajectory for paretic RLN vocal fold motion. α = jet deflection angle, Ψ = total included divergence angle for unimpaired motion (30°).

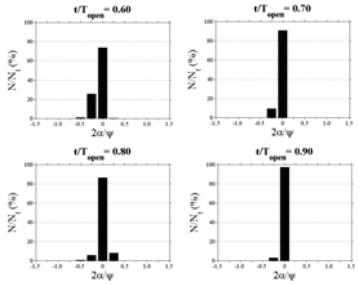

Figure 5: Glottal jet trajectory for paralyzed RLN vocal fold motion. α = jet deflection angle, Ψ = total included divergence angle for unimpaired motion (30°).

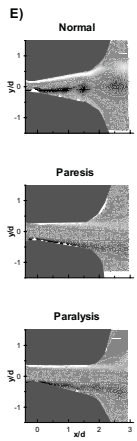

Figure 6: Vorticity magnitude at t/T_{open} = 0.70.

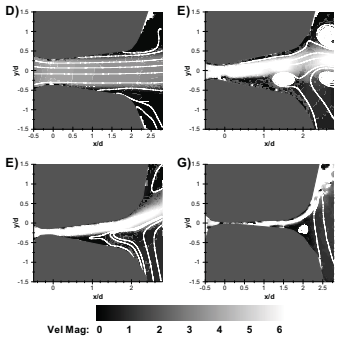

Figure 7: Velocity contours for normal vocal fold motion.

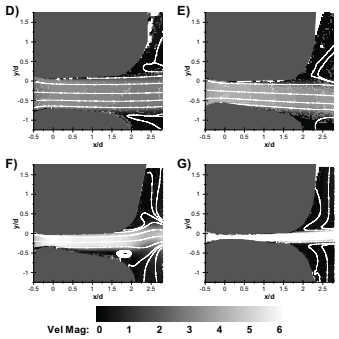

Figure 8: Velocity contours for paretic vocal fold motion.

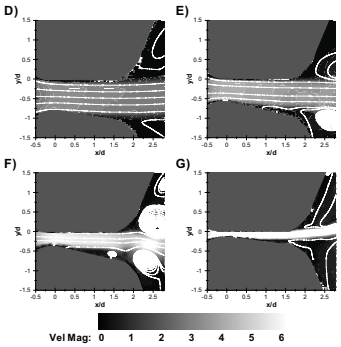

Figure 9: Velocity contours for paralyzed vocal fold motion.

Table 2: Transglottal pressure drop as a function of jet deflection angle.

	ΔP [cmH_2O]	σ^2 [cmH_2O]	Change [%]
Normal Motion			
θ = 0 (unattached)	10.197	1.318E-3	0.00
θ = -12.5 (attached)	10.321	8.362E-4	1.21
Paretic Motion			
θ = 0 (attached)	9.848	1.487E-3	3.32
θ = -7.5(unattached)	9.521	4.310E-3	0
Paralyzed Motion			
θ = 0 (attached)	9.098	1.755E-3	0.45
θ = -3.75 (unattached)	9.057	9.498E-4	0.00